

Highlights

Characterization of the M1 and M2 layers in the undisturbed Martian ionosphere through solar minimum leading to solar maximum with MAVEN ROSE

Jennifer Segale, Marianna Felici, Paul Withers, Shannon Curry

- There is more seasonal variability in the dawn ionosphere than the dusk ionosphere;
- The M1 layer is present at small SZA and, when present, is located ~ 20 km below the M2 layer;
- The ratio of M1 over M2 peak densities increases with SZA, and the two layers get farther from one another.

Characterization of the M1 and M2 layers in the undisturbed Martian ionosphere through solar minimum leading to solar maximum with MAVEN ROSE

Jennifer Segale^a, Marianna Felici^b, Paul Withers^{a,b}, Shannon Curry^c

^a*Astronomy Department, Boston University, 725 Commonwealth Avenue, Boston, 02215, MA, USA*

^b*Center for Space Physics, 725 Commonwealth Avenue, Boston, 02215, MA, USA*

^c*Laboratory for Atmospheric and Space Physics, University of Colorado Boulder, 1234 Innovation Drive, Boulder, 80303, CO, USA*

Abstract

We utilise data from the MAVEN Radio Occultation Science Experiment (Withers et al., 2020) - with unprecedented coverage in solar zenith angle - to isolate the effects that local time and season induce on the photochemical ionosphere of Mars around solar minimum, leading to solar maximum. 219 out of the 1228 electron density profiles of the Martian undisturbed - by solar events or dust storm - dayside ionosphere collected by MAVEN ROSE between July 2016 and December 2022 show a distinct M1 layer below the M2 layer. This allowed us to study the behavior of both the M2 and M1 peak densities and altitudes as a function of solar zenith angle, and, for the first time, to be able to separate these trends in dusk and dawn local time, as well as by Southern Spring and summer versus Southern Fall and Winter. We find that the M1 layer at small SZA can occur at altitudes lower than 100 km; that the peak altitudes and densities of both the M2 and M1 layers at dawn change more with season than they do at dusk; and that the M2 peak density decreases at a faster rate than the M1 with SZA.

Keywords: Martian Ionosphere, M1 layer, M2 layer

1. Introduction

Historically, radio occultation observations have been a well utilised method to study planetary ionospheres, especially the ionosphere of Mars, because of

their broad vertical coverage, good vertical resolution, and low density uncertainty (e.g., Withers et al., 2020, and references therein). Electron density profiles of the Martian dayside ionosphere generally show two peaks, with one of lesser density just below the other. Each peak indicates a different layer. The upper layer is referred to as the M2 layer, while the lower layer is called the M1 layer.

The M2 layer is where the largest electron density peak occurs and is usually located at an altitude between about 120 and 180 km (e.g., Bougher et al., 2017). The M2 layer is produced by ionization due to extreme ultraviolet (EUV) photons. In general, as solar zenith angle (SZA) increases, the peak electron density value in the M2 layer decreases, while the altitude of the peak increases (e.g., Fallows et al., 2015, and reference therein). This trend follows closely the one expected from an idealized photochemical theory (Chapman, 1931a,b). The M1 layer is situated below the M2 layer. The M1 layer appears on electron density profiles as a small peak or shoulder below the M2 peak, but is not always present or visible, and its behavior is less understood [Withers 2023, SUBMITTED]. The M1 layer forms by ionization from soft X-rays and Auger electrons, as opposed to EUV photons for the M2 layer (e.g., Bougher et al., 2017). Similar to the M2 layer, the peak electron density of the M1 layer decreases as the SZA increases. The altitude of the peak increases as SZA increases, as it does for the M2 layer, but previous studies, conducted during solar maximum, show this change occurring at a slower rate than it does for the M2 layer (Fallows et al., 2015, and references therein).

The peak altitudes and densities of the M1 and M2 layers change depending on various factors, such as phase in the solar cycle (e.g., Withers et al., 2023): while the scale height above the M2 peak in the photochemical ionosphere is quite similar going from solar maximum to solar minimum, the M1 and M2 peak densities increase from solar minimum to solar maximum, because of the increased solar irradiance. Other factors that can affect the M1 and M2 layers, and the ionosphere in general, include solar activity (e.g., Hantsch and Bauer, 1990) [Felici, COMPANION MANUSCRIPT], solar flares (e.g., Mendillo et al., 2006), dust storms (Kliore et al., 1972; Felici et al., 2020)[Felici, COMPANION MANUSCRIPT], and local time sector (e.g., Pilinski et al., 2019; Felici et al., 2022). The changes that these factors induce on the peak densities and altitudes are better characterized for the M2 layer, and less studied for the M1 layer (e.g., Fox and Yeager, 2006, 2009; Fallows et al., 2015, and references therein) [Withers 2023, SUBMITTED].

The nightside ionosphere, beyond the terminator, will not be considered in this study, aside from helping determine the location of the terminator: photoionization is absent on the deep nightside, and instead horizontal transport of dayside photo-produced plasma and ionisation due to precipitating particles are the origin of electron densities larger than zero that can be detected beyond the terminator (e.g., Withers et al., 2012; Němec et al., 2010).

Previous studies that used dayside radio occultation data - very few of which focused on the M1 layer - have found some variation in both M1 and M2 peak densities and altitudes at similar SZAs (e.g., Yao et al., 2019; Fallows et al., 2015) consistent with what is expected in an idealised photochemical theory (Chapman, 1931a,b), and their extrapolation of subsolar peak altitude and density led to different results (e.g., Nielsen et al., 2006; Morgan et al., 2008; Fox and Yeager, 2009; Fox and Weber, 2012), some of which we report in Tables 3 and 4 to contextualise our results in Section 3; however, while longitudinal and thermal tide dependence (Bougher et al., 2004; Fox and Weber, 2012), and irradiance dependence (e.g. Fox and Yeager, 2009) were previously considered, the M1 and M2 peak density and altitude changes with SZA were never, to our knowledge, separated in local time sector or season to quantify their dependence on these factors, which we expect have an effect (e.g., Pilinski et al., 2019; Felici et al., 2022) on the idealised photochemical ionosphere (Chapman, 1931a,b; Fallows et al., 2015) (please see Section 2). In other words, we expect that at fixed solar zenith angles, the ionosphere at southern spring and summer will be different from the ionosphere at southern autumn and winter, and the ionosphere at dawn will be different than the ionosphere at dusk. We utilise M1 and M2 peak densities and altitudes as proxies to quantify "how different" the ionosphere is in such circumstances. Additionally, quantitatively characterising the changes that local time and season induce on the Martian ionosphere when undisturbed - namely no solar events or dust storms are affecting the ionosphere - is paramount to understanding and quantifying ionospheric variability in the presence of external triggers and during a more active phase of the solar cycle.

The thorough SZA coverage of the Radio Occultation Science Experiment (ROSE) (Withers et al., 2020) allowed us to make comparisons between the M1 and M2 layers under different solar longitude (L_S) and local solar time (LST) conditions and investigate how the M1 and M2 peak altitude and density change, independently and relative to one another.

The Radio Occultation Science Experiment (ROSE) (Withers et al., 2020)

was added to the MAVEN (Jakosky et al., 2015) science payload in 2016. Since then, ROSE has collected more than 1000 electron density profiles, and a good number of these show both M1 and M2 layers. While geometric constraints limit radio occultation observations at Mars to Solar Zenith Angles (SZA) between $\sim 45^\circ$ and $\sim 136^\circ$, making it impossible for this technique to observe subsolar peak altitudes (e.g. Hinson et al., 1999; Tamburo et al., 2023), ROSE has been able to cover that range nearly completely down to $\sim 47^\circ$ [Withers et al. 2023, SUBMITTED], in addition to a comprehensive coverage in latitude and longitude.

The focus of this study is on the effects that Local Solar Time (LST) - dawn versus dusk local time sectors - and season - dust season near perihelion versus non-dust-season near aphelion - have on the trends that peak altitude and density are expected to have with SZA from the idealized photochemical theory. To better isolate these effects, we focus on the "undisturbed" ionosphere: when there are no known events external to the ionosphere (e.g. ICMEs, dust storms) causing perturbations. We expect the dusk ionosphere, exposed for longer to light, to be different, and extend to higher SZA angles, than the dawn ionosphere, that it is just coming out from night. We also expect dust season to have effects on the ionosphere: at perihelion, in fact, some amount of dust is lofted in the atmosphere, regardless of whether or not there are dust storms (Montabone et al., 2020).

Because of the effects that increased solar irradiance can have on ionospheric conditions, we feel it is important to note the phases of the solar cycle in which data was obtained. The ROSE electron density profiles utilised in this study were collected during the less active half of the solar cycle, from just before solar minimum to just before solar activity ramps up approaching solar maximum (see Figure 4 for a visualization of when data was acquired).

This paper is organised as follows: in Section 2 we will illustrate how the data was filtered and analyzed; in Section 3 we will report and discuss the results of this study; in Section 4 we summarize and report our conclusions.

2. Methods

We began by manually examining 1228 electron density profiles collected by MAVEN ROSE (Withers et al., 2020) between July 2016 and December 2022. The data covered a SZA range between $\sim 47^\circ$ and $\sim 136^\circ$, latitudes from -85.4° to 88.9° , and had comprehensive coverage in longitudes and L_S .

We applied four criteria to select the profiles which would be included in this study. First, even though ROSE profiles collected in 2023 were available on the PDS when this manuscript was written, we limited this study to the lower part of the solar cycle, only approaching the higher solar activity of solar maximum. This choice allowed to include enough profiles distributed in the LST and L_S sectors we wanted to study, while avoiding high solar activity that caused noticeable outliers in the data.

Second, we chose to include in this study only profiles that we deemed "complete" in altitude, namely profiles with full altitude coverage between 75 km and 250 km, in order to have a complete view of predicted altitudes for the M1 and M2 layers. Additionally, coverage of altitudes above the main ionospheric layers allows for better baseline corrections during the process of generating electron density profiles, making these profiles more reliable for determining M2 and M1 peak altitudes and densities (Withers et al., 2020).

Third, because the purpose of this work is to characterize the variability of both the M2 and M1 layers, the profiles which did not display an M1 layer were set aside. Therefore, we categorized "complete" profiles into three categories: *strong* (example in Figure 1, green), *medium* (example in Figure 1, yellow), and *none* (example in Figure 1, brick red). The profiles that display an obvious, well-defined M1 layer fall into the *strong* category. In the *medium* category belong profiles that display an M1 layer as a shoulder rather than a distinct peak, or where there was some ambiguity in distinguishing a local point of maximum density. In these cases the location of the M1 peak is less certain. In the *none* category fall all the profiles that show no visible M1 peak. Only electron density profiles in the *strong* and *medium* categories were further examined.

An interesting result of this categorization process is that all profiles used (i.e. those in the *strong* and *medium* categories) have $SZA < 110^\circ$. This means that there were no profiles in this dataset with both M1 and M2 layers at $SZA > 110^\circ$. Ionospheric structure seems to transition from dayside structure with M1 and M2 layers to nightside structure around this SZA. This also gives us an idea of how far past the terminator ($SZA = 90^\circ$) the dayside extends (e.g., Withers et al., 2012; Němec et al., 2010), and if that transition occurs at different SZA at dusk compared to dawn. In other words, we would expect the dayside ionosphere at dusk to extend at $SZA > 90^\circ$ because the ionosphere at dusk has been exposed to sunlight for longer than it was at dawn, and, therefore, it would take more time without direct sunlight for it to estinguish. From Figures 5 and 10 from Felici et al. (2022)

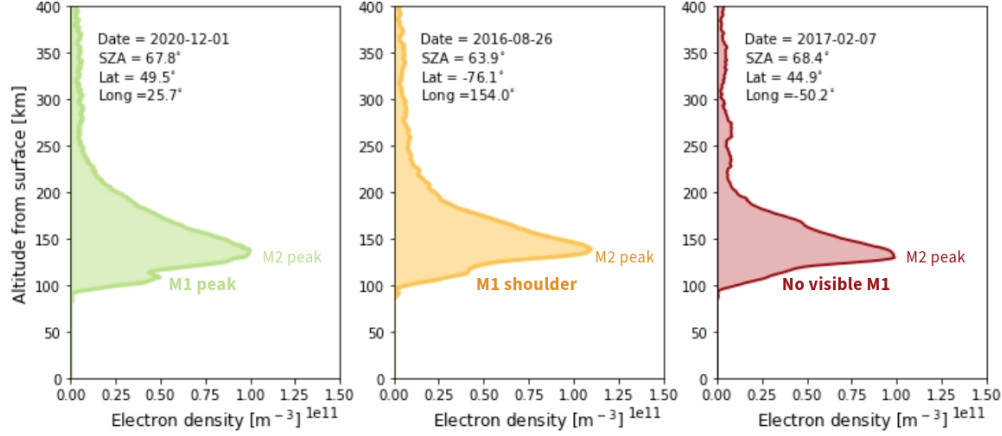


Figure 1: Examples of ROSE electron density profiles for the *strong*, *medium*, and *none* categories. Left is the *strong* profile (green), with a well-defined peak below the M2 layer. Middle is the *medium* profile (yellow), in which the M1 shows more as a shoulder rather than a peak. Right is the *none* profile (brick red), with no discernible M1 peak or shoulder.

we can appreciate how, at the altitudes examined in this study, the electron density drops from $\sim O(10^{11})$ to $\sim O(10^{10})$ within $\pm 2^\circ$ SZA at all altitudes, once we pass the terminator.

The first three criteria alone significantly decreased the number of profiles suitable for this study from 1228 to 360. For these, we recorded the peak altitudes and densities of both the M1 and M2 layers with errors. To get these values, we identified the peaks visually by inspecting each profile. As previously mentioned, the *medium* profiles do not display a clear peak, but a shoulder or a cluster of smaller peaks. Therefore, errors on the M1 peak in the *medium* profiles were measured as the distance between two near local maxima or as the width of a shoulder. The errors on the *strong* profiles were recorded as the instrument error for the density, namely $5 \times 10^9 \text{ m}^{-3}$, and as the vertical resolution of 1 km in altitude (Withers et al., 2020). In Figure 2, top, we report peak altitude as a function of SZA for both the M1 and M2 layers in these 360 observations. In order to clearly visualise the distribution of this dataset and compare the distribution of the M1 layer (Figure 2, bottom) to the one of the M2 layer (Figure 2, middle), we utilize box plots, showing the minimum (bottom bar), first quartile (Q1, bottom

of the box), median (horizontal line), third quartile (Q3, top of the box), and maximum (top bar) of each 5° -wide bin of the data. We indicate the interquartile range as IQR. Outliers are indicated with diamond shapes above or below a box and correspond to data outside the maximum and minimum values interval, which is defined as the range between Q1 minus 1.5IQR and Q3 plus 1.5IQR $[(Q1-1.5\text{IQR}), (Q3+1.5\text{IQR})]$. We chose a bin width of 5° SZA to strike a balance between SZA resolution, showing the spread in the data, and reducing scatter to find if a trend existed in the median. While some of the bin populations are small, especially at the lowest and highest SZAs, we felt that these data were still valuable because they provide a sense of the general trend, particularly for low SZAs where there has not been a lot of prior study. Five features capture our attention in Figure 2: a) the IQRs of the M1 (red) tend to be as large on average as the IQRs of the M2 (blue), which means a similar spread in altitude distribution for the values of the M1 peak compared to the M2, when the M1 is present; b) the median of the boxes for both the M1 and M2 follow the expected trend for an idealised photochemical theory, except for the bin centered on 52.5° , which includes data collected when both solar events and dust storms were disturbing the ionosphere (see Felici et al., COMPANION MANUSCRIPT for more details); c) the bin centered on 57.5° presents a much larger box than its neighbors' boxes, for similar reasons as those listed in point two. d) the drop in the median value in the bin centered on 97.5° signals the transition to the nightside ionosphere. e) in general, there are more outliers in the M1 values than in the M2 values, however we consider this number of outliers ($\sim 3\%$ of the 360 profiles) normal and not a cause for concern. We show in Figure 3 the same plot as Figure 2, but for peak densities of the M2 and M1 layers as a function of SZA. Besides similar considerations to the ones we made for features a) to d) in Figure 2, it seems that peak densities for both the M1 and M2 present larger spread at low SZA, and smaller spread at higher SZA, when they inevitably start converging to a lower order of magnitude, consistent with what was found in previous studies (e.g., Felici et al., 2022).

The fourth, and last, criterion to filter the data examined in this study was excluding from this study ROSE data collected during known dust storms and known solar events. We want to remind the reader that the objective of this study is to characterize how the undisturbed Martian ionosphere changes with SZA, but also with L_S and LST, in order to obtain an accurate baseline for the ionosphere around solar minimum. This is paramount to fully un-

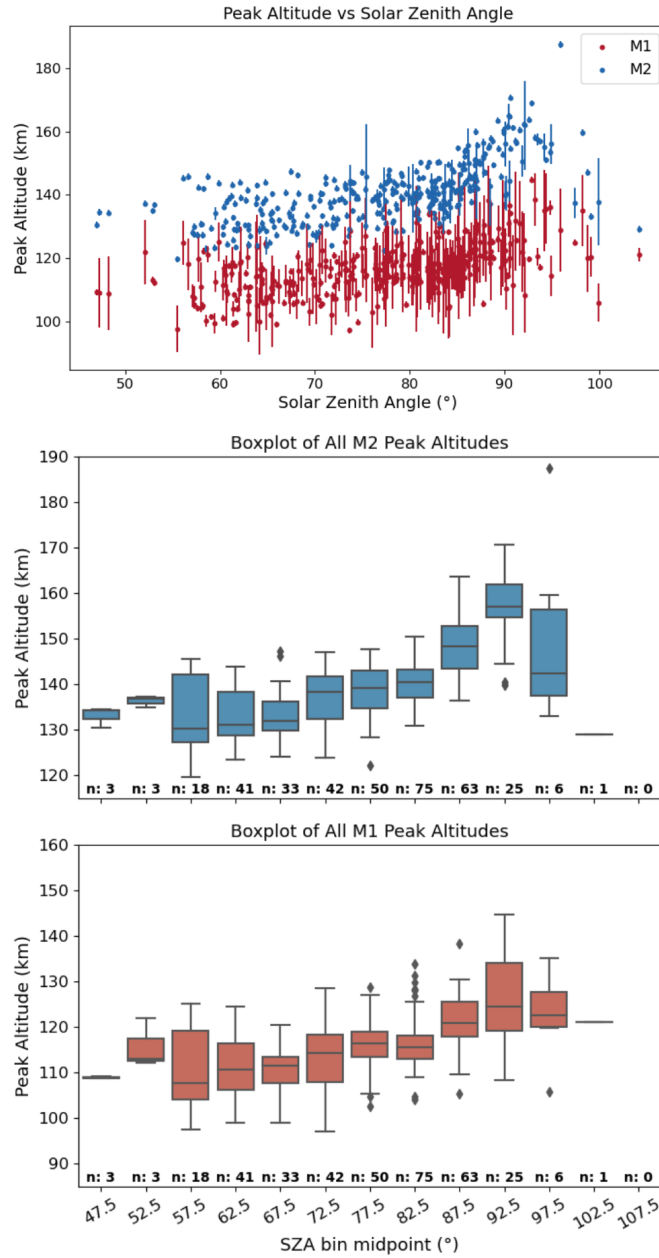


Figure 2: Top: M1 (red) and M2 (blue) peak altitudes of 360 electron density profiles selected using criteria one to three previously listed as a function of SZA; middle: boxplot of the 360 M2 peak altitudes in 5° SZA bins. We indicated number of profiles that fall in each bin at the bottom of the plot; bottom: boxplot of the M1 peak altitudes in 5° SZA bins, with center value of the bin reported on the x axis.

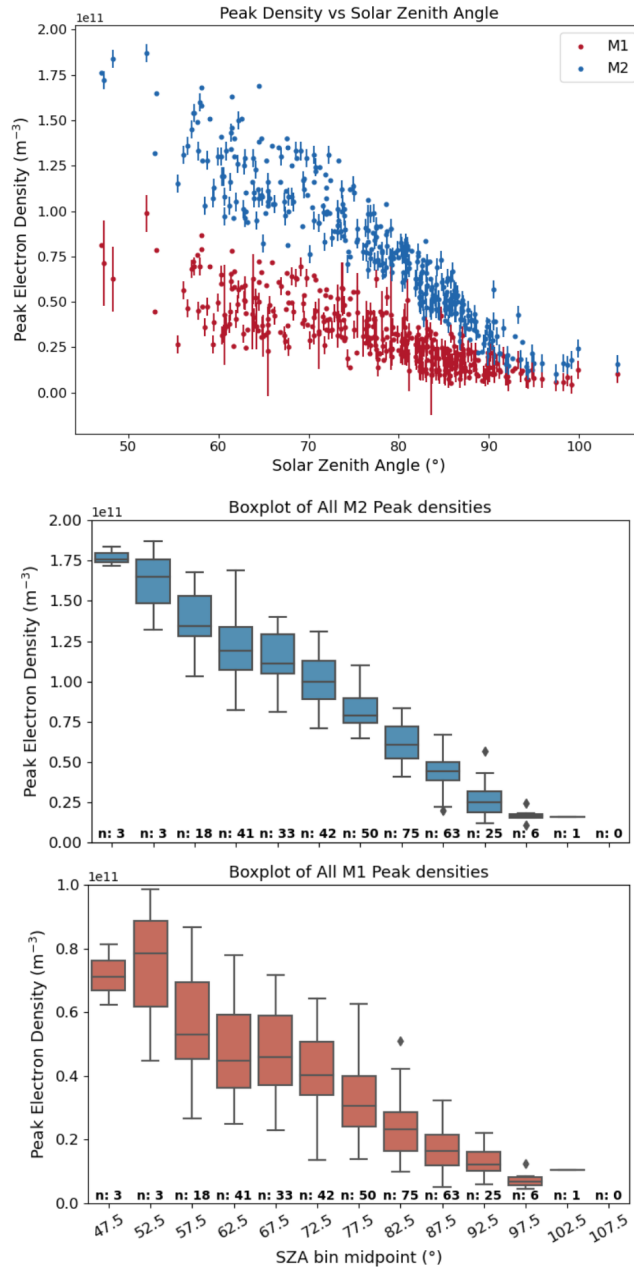


Figure 3: Top: M1 (red) and M2 (blue) peak densities of 360 electron density profiles as a function of SZA; middle: boxplot of the 360 M2 peak densities in 5° SZA bins. We indicated number of profiles that fall in each bin at the bottom of the plot; bottom: boxplot of the M1 peak densities in 5° SZA bins.

derstand the behavior of the Martian ionosphere, and be able to accurately quantify the effects that events external to the ionosphere (e.g. ICMEs, dust storms) have on the ionosphere. To achieve our objective, firstly, we excluded from this study profiles collected during known dust storms in MY 33, 34, 35, and 36, as those are known to heavily affect peak altitudes (Felici et al., 2020, and references therein); secondly, we excluded profiles collected during known solar events; solar events can affect electron densities in the ionosphere, however, their effect on the lower ionosphere has not been fully characterized [see Felici et al., COMPANION MANUSCRIPT]. To appreciate the spread that these kinds of events can introduce in the data, please notice the medians for both the M1 and M2 peak altitudes (Figure 2) and densities (Figure 3) and their deviation from the trends expected from an idealized photochemical theory, as previously discussed.

The number of ROSE electron density profiles which satisfied all four of these criteria is 219, with which we will show how the ratio between M1 and M2 peak densities and the difference between the M2 and M1 peak altitudes change with SZA (see Section 3). Additionally, we separated these 219 profiles into four groups based on their Local Time (LST) and Solar Longitude (L_S). At dusk, the Martian atmosphere has been exposed to the Sun for several hours, while for the dawn atmosphere the Sun has just risen, and depending on where Mars is in its orbit, the planet will be exposed to different solar flux and heat when it is at its farthest point from the Sun (aphelion) than when it is at its closest point to the Sun (perihelion). In this study, we defined dawn as the LST between 0 and 12, and dusk as the LST between 12 and 24. We defined L_S from 341° to 360° and 0° to 161° as "near aphelion", and from 161° to 341° as "near perihelion". For simplicity, in the rest of the paper, we will refer to the four groups in which the 219 ROSE electron density profiles were split as dawn aphelion, dawn perihelion, dusk aphelion, and dusk perihelion. Each group covers a different range of SZAs. We summarize the nomenclature, the LT, L_S , and SZA ranges of these four groups in Table 1. In Figure 4 we report the distribution of the profiles in each of these groups in LT sector, L_S season, SZA, and phase in the solar cycle to show the relatively similar dawn-dusk coverage, albeit with some differences in SZA sampling for the same time of the year.

For each of the four categories, the M1 and M2 peak densities and peak altitudes were fitted as a function of SZA with functions describing the behaviour of an ideal photo-chemically produced ionosphere (Chapman, 1931a,b), similarly to the methodology that Fallows et al. (2015) utilised with the MGS

Table 1: Ranges in LST and L_S defining the four groups in which we split the data, and name with which we will refer to these categories in this paper.

Name in this paper	Local Time (LST)	L_S [$^\circ$]
dawn - aphelion	00:00 - 12:00	0-161 and 341-360
dawn - perihelion	00:00 - 12:00	161 to 341
dusk - aphelion	12:00 - 24:00	0-161 and 341-360
dusk - perihelion	12:00 - 24:00	161 to 341

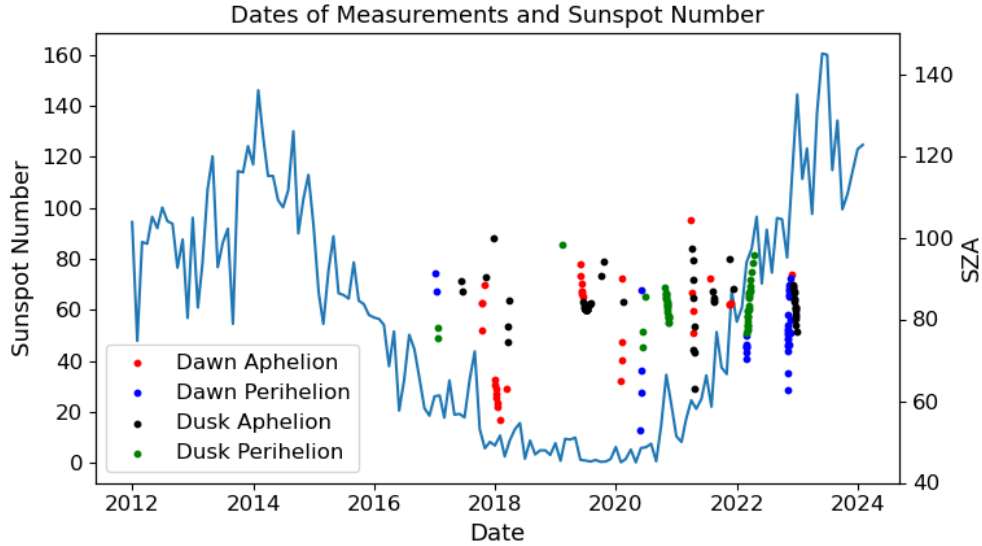


Figure 4: Distribution of the 219 ROSE electron density profiles which satisfied our criteria, divided into four categories -dawn aphelion, dawn perihelion, dusk aphelion, and dusk perihelion - as a function of time and relative Sun Spot Number (SSN) and SZA. The y axis for the ROSE data is on the right, labelled SZA, and the y axis for the sunspot number is on the left. The source for the sunspot number is WDC-SILSO, Royal Observatory of Belgium, Brussels.

dataset. The fit parameters so obtained were compared for the four categories (dawn aphelion, dawn perihelion, dusk aphelion, and dusk perihelion) to quantify the effects of LST and L_S on the Martian photo-produced dayside ionosphere. However, the MGS dataset had a much narrower SZA coverage ($\simeq 70^\circ$ to $\simeq 90^\circ$) than the one of ROSE, and only limited to northern latitudes, unlike ROSE. Therefore, for the peak altitude, from Fallows et al. (2015), to fit data with $\text{SZA} \leq 90^\circ$ and extrapolate it to higher and lower SZA, we utilized the function

$$z_m = z_0 + L \times \ln(\text{Ch}(\chi)) \quad (1)$$

where m stands for either the M1 or the M2 peak, z_m is the altitude of the peak, z_0 is the fitted sub-solar altitude of the peak, χ is the SZA, and L is the fitted lengthscale which should coincide with the scale height of the neutral atmosphere, where an idealized photochemical theory applies. $\text{Ch}(\chi)$ is a correction factor (Chapman, 1931b; Smith III and Smith, 1972; Fallows et al., 2015) that corresponds to the altitude predicted by the ideal Chapman theory at a SZA of χ° . It reduces to $\sec(\chi)$ at small SZA, returning the equation to the more familiar format reported by Hantsch and Bauer (1990).

For fitting the peak density, we used

$$N_m = N_0 \left(\frac{1}{\text{Ch}(\chi)} \right)^k \quad (2)$$

where m stands for either the M1 or the M2 peak, N_m is the density of the peak, N_0 is the fitted sub-solar density of the peak, χ is the SZA, and k is the fitted exponent. Here $\text{Ch}(\chi)$ corresponds to the Chapman density predicted at χ° SZA.

Only datapoints with SZA 90° or below were used in the fitting calculations, as ionospheric structure begins to change as SZA increases past this point. We found that fitting with datapoints at greater SZA caused the models to deviate from the data at SZA just less than 90° . Excluding these points at $\text{SZA} > 90^\circ$ from the fitting calculations allowed us to find the models that best fit the majority of the data.

We report our results in the next Section (Section 3).

3. Results and Discussion

After filtering, the 219 remaining profiles have slightly different coverage of SZA, Mars latitude and longitude, and local time than before. These

Table 2: Summary of the local time, latitude, longitude, and SZA coverage in each category of the 219 profiles used.

Category	Local Time (LST)	Mars Lat [°]	Mars Long [°]	SZA [°]
dawn - aphelion	0.607222 - 11.9892	-63.6 - 88.9	-160.5 - 170.4	55.5 - 104.2
dawn - perihelion	4.41278 - 11.9656	-65.4 - 74.5	-178.2 - 171.8	52.9 - 91.2
dusk - aphelion	12.6456 - 22.6533	-77.4 - 85.8	-154.2 - 177.0	63.2 - 99.9
dusk - perihelion	12.2978 - 21.2856	-67.9 - 75.2	-166.6 - 168.9	73.2 - 98.3

ranges are summarized in Table 2. Each category covers a broad range of SZAs, with dusk perihelion having the smallest range of about 25° . Each group also covers about 150° of Mars latitude and about 330° of Mars longitude, meaning that we have data over most of the surface of Mars. Local time coverage also appears fairly broad in each group, meaning there are no clusters of data around particular times.

In Figure 5, top, we report the boxplot distribution of the ratio between the M1 peak density over the M2 peak density, indicating both mean (triangle) and median (horizontal line) for a total of 219 profiles. In Figure 5, bottom, we report the distribution of the difference between the M2 peak altitude and the M1 peak altitude, for a total of 219 profiles. We did not split the 219 profiles into the four groups reported in table 1, as we found that this made bin populations in some cases too small to be able to build a full picture for these two proxies (ratio of densities and altitude difference). Leaving these data uncategorized causes a greater spread than there would be otherwise, which introduces a few outliers in each plot, but as these outliers are only a small portion of the dataset we do not think they are a cause for concern. From 5, top, we can observe that the ratio between the M1 peak densities tends to generally increase with SZA, indicating that the density of the M2 layer drops at a higher rate than the M1 density does, making the M1 more prominent at higher SZA. However, some bins at low SZA are less populated than the bins for $SZA > 72.5$, and bins < 62.5 are populated only by data collected in the dawn sector, therefore might not be representative of the average trend of these proxies (see 7 and relative text). From 5, bottom, the two layers are generally farther apart with increasing SZA, and similar considerations as the ones we did for the ratios can be made here (see Figure 6 and relative text).

In Figure 6 we show the M1 (bottom) and M2 (top) peak altitudes for the four groups dawn aphelion, dawn perihelion, dusk aphelion, and dusk

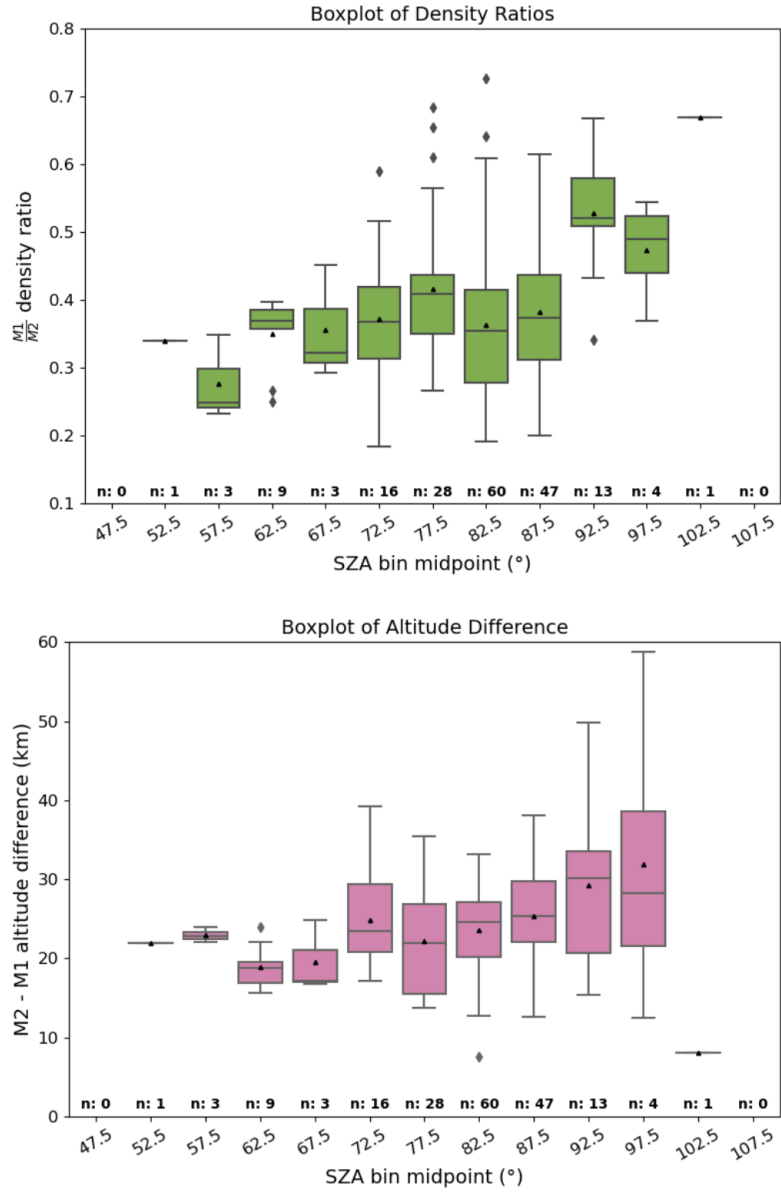


Figure 5: At the top, box plot of the ratio between the M1 peak density and the M2 peak density. At the bottom, box plot of the M2 and M1 peak altitude difference. In both plots we indicate both mean (triangle) and median (horizontal line).

perihelion, and the relative fitted curves, with fit parameters reported in the legend of Figure 6 and in Table 3 in the context of other studies. For the M1 layer, dusk aphelion seems an outlier compared to the other trends: in the M1 peak altitude data, the dusk aphelion fit is elevated significantly from the other categories, and has a much smaller rate of change with SZA. This may be due to a lack of data in this category between 50 - 70° SZA. Most of the data for this category are concentrated between 80 - 90° SZA. This means that the data we have may not be representative of lower SZAs and the fit there may be more inaccurate. Any higher than normal data points would have a greater effect on the fit. Our results suggest that dawn aphelion is the group that presents consistently -for both M1 and M2- the lowest peak altitude, quite separated from dawn perihelion (more on this later). The L fit parameter is consistent with a scale height of 10 km from an idealized photochemical theory for the M2 layer, higher than the values obtained by Fallows et al. (2015), and closer to those of Fox and Weber (2012). The MGS data Fallows et al. (2015) utilised was more limited in SZA (only between 70 and 90°), the observations were collected at a different phase of the solar cycle (solar maximum), and effects of dust and solar events were not removed from the dataset: that is to say that we expect photo-produced ionospheric layers to behave according to an idealized photochemical theory, whereas we do not expect that the effects other phenomena have on M1 and M2 peak altitude and densities to be SZA dependent. This discrepancy in values between our L fit parameters and those obtained by Fallows et al. (2015) suggests that effects on the ionosphere from solar maximum, dust storms, and solar events "mitigate" the trend the M2 and M1 peak altitude would have as a function of SZA. Similar considerations can be made for the discrepancies with Fox and Weber (2012), who also utilised MGS data. We also want to highlight that peak altitudes for the M1 layer can fall below 100 km, making it impossible to detect for the altitude coverage of the Viking probe, supporting the hypothesis Withers et al., [2023, SUBMITTED] make.

In Figure 7 we show the M1 (bottom) and M2 (top) peak densities for the four groups dawn aphelion, dawn perihelion, dusk aphelion, and dusk perihelion, and the relative fitted curves, with fit parameters reported in the legend of Figure 7 and in Table 4 in the context of other studies.

As for peak densities, dawn aphelion is the lowest curve, with densities well below those of dawn perihelion, while the two seasons are consistent within error for both the M1 and M2 for dusk. In other words, between aphelion and perihelion, the dawn LST sector is the one that shows the

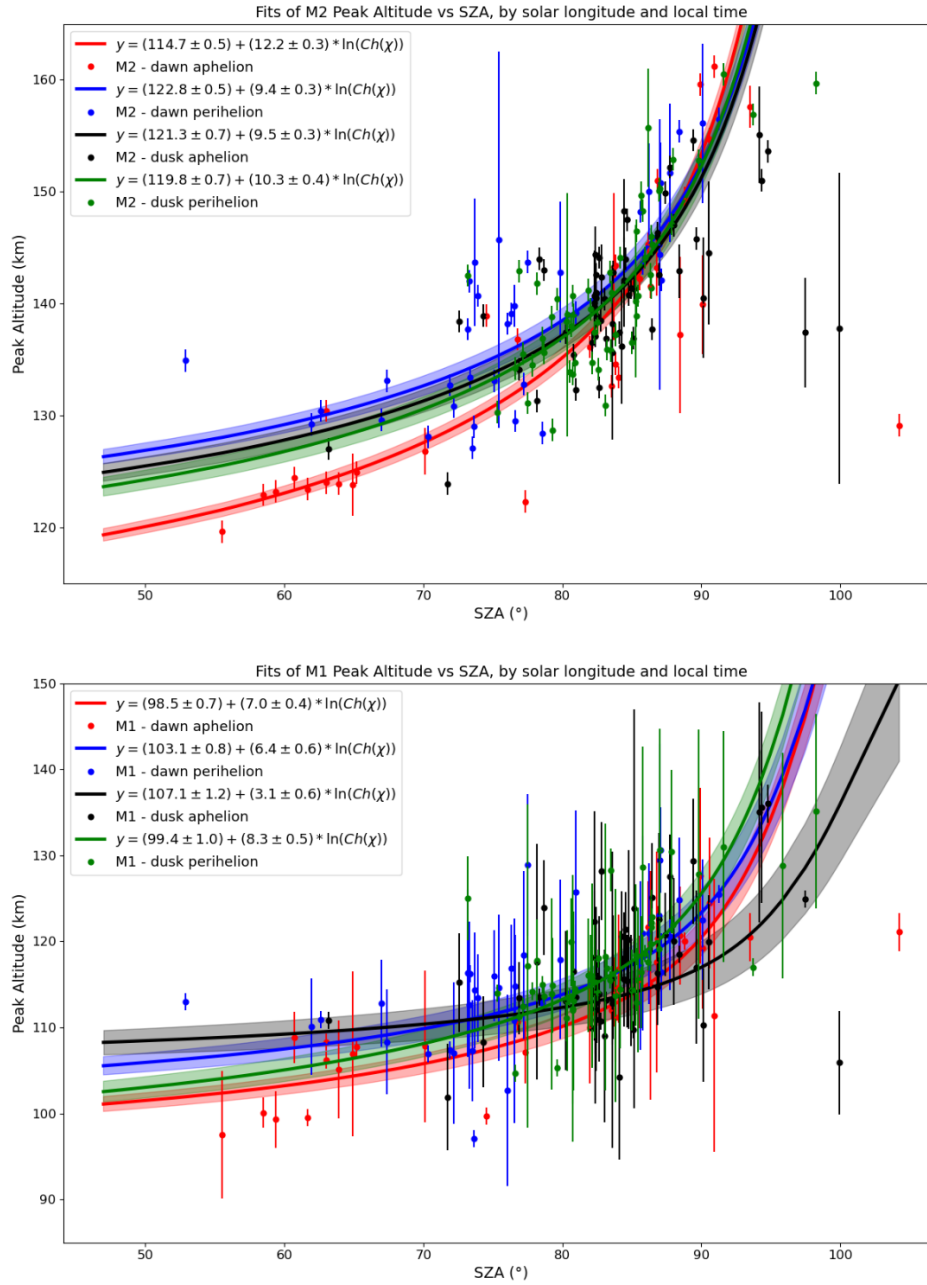


Figure 6: Fit for M1 (bottom) and M2 (top) peak altitudes for the four groups dawn aphelion, dawn perihelion, dusk aphelion, and dusk perihelion, with the results for the fit parameters printed in the legend, and in Table 3 for clarity.

Table 3: Fit parameters for M1 and M2 peak altitudes extrapolated to the subsolar point from this study, and comparison with previous studies by other authors. We indicated with This Work with TW, for short.

Source	M2 Z ₀ [km]	M1 Z ₀ [km]	M2 L [km]	M1 L [km]
Fox and Weber (2012)	125	109	7.2	4.0
Fallows et al. (2015)	130.9 ± 1.8	104.9 ± 1.8	5.2 ± 1.5	2.5 ± 1.5
TW - dawn aphelion	114.7±0.5	98.5 ± 0.7	12.2±0.3	7.0 ± 0.4
TW - dawn perihelion	122.8±0.5	103.1±0.8	9.4±0.3	6.4±0.6
TW - dusk aphelion	121.3±0.7	107.1±1.2	9.5±0.3	3.1±0.6
TW - dusk perihelion	119.8±0.7	99.4±1.0	10.3±0.4	8.3±0.5

largest difference in peak density. This is consistent with what Felici et al. (2022) postulated from comparing MAVEN ROSE and MAVEN LPW electron density at dawn and dusk: the two datasets were consistent within error at dusk, but not at dawn; that study utilised only data collected between 0-180° L_S, shifted from the range we considered for aphelion in this study (see Table 1) of about 20°, possibly capturing some of the effects that dust season itself induces on peak altitudes and densities at dawn. Moreover, the higher peak densities close to perihelion are consistent with measurements of solar electron content which follows seasonal periodicity and peaks at L_S ~ 240 (Sánchez-Cano et al., 2018), namely at Northern Autumn and Southern Spring.

Peak densities and altitudes for both the M1 and M2 layers are lower than what Fallows et al. (2015) found in their study at aphelion and can be consistent within error at perihelion (with a caveat on the M1 peak altitude at dusk aphelion). The MGS data utilised by Fallows et al. (2015) in their studies was collected during solar maximum, and at higher latitudes, suggesting that either at solar minimum electron densities are lower and the M1 and M2 peak densities occur at lower altitudes, or that latitudes (and differences in crustal field strength and configuration) could also affect electron densities in the lower ionosphere. However, while the first statement is consistent to what Withers et al. (2023) found, the second statement is not consistent with what Flynn et al. (2017) found, suggesting the first explanation is the most plausible. Similar considerations can be made for the discrepancies with Fox and Yeager (2006, 2009), who also utilised MGS data. As for the estimate of Němec et al. (2011), possibly from a similar phase of the solar cycle, their estimate was conducted over more than 30000 Mars

Table 4: Fit parameters for M1 and M2 peak electron densities extrapolated to the sub-solar point from this study, and comparison with previous studies by other authors. We indicated This Work with TW, for short.

Source	M2 N_0 [10^{11} m^{-3}]	M1 N_0 [10^{10} m^{-3}]	M2 k	M1 k
Fox and Yeager (2006)	1.82 ± 0.03	9.4 ± 0.4	0.46 ± 0.01	0.55 ± 0.02
Fox and Yeager (2009)	1.9 ± 0.03	8.7 ± 0.3	0.49 ± 0.01	0.50 ± 0.03
Němec et al. (2011)	1.59 ± 0.016	-	0.546 ± 0.001	-
Fallows et al. (2015)	1.97 ± 0.07	7.7 ± 0.7	0.54 ± 0.04	0.55 ± 0.08
TW - dawn aphelion	1.51 ± 0.04	4.38 ± 0.36	0.53 ± 0.02	0.43 ± 0.06
TW - dawn perihelion	1.93 ± 0.05	6.74 ± 0.45	0.53 ± 0.02	0.45 ± 0.05
TW - dusk aphelion	1.69 ± 0.09	5.71 ± 0.76	0.62 ± 0.03	0.52 ± 0.07
TW - dusk perihelion	1.79 ± 0.10	7.19 ± 0.99	0.53 ± 0.03	0.53 ± 0.07

Express - MARSIS profiles, therefore averaging several effects.

Finally, extending beyond $SZA \sim 90^\circ$, we see mostly data collected at dusk, both perihelion and aphelion, suggesting that our hypothesis might be correct: the dusk ionosphere tends to persist longer beyond the terminator than the dawn does. We want to be cautious, however, given that there might be a sampling bias, and more data needs to be collected to make definitive statements.

4. Summary and Conclusions

219 electron density profiles of the Martian undisturbed dayside ionosphere collected by MAVEN ROSE between July 2016 and December 2022, through solar minimum leading to solar maximum, show clear M2 and M1 layers. We used these 219 profiles to characterize how M2 and M1 peak electron densities and altitudes change with SZA, LST sector - dawn vs dusk - and season -aphelion (Southern Autumn and Winter) vs perihelion (Southern Spring and Summer). Therefore, we split these 219 profiles into four groups: dawn aphelion, dawn perihelion, dusk aphelion, and dusk perihelion. For the frequency with which the ionosphere is sampled with ROSE data, quite different from MGS RO (Bougher et al., 2004), and for the difference in latitudinal sampling from MGS, tidal effects were not considered in this study.

We find distinct differences between the different groups of data. The biggest difference, both in peak densities and in peak altitudes, is found be-

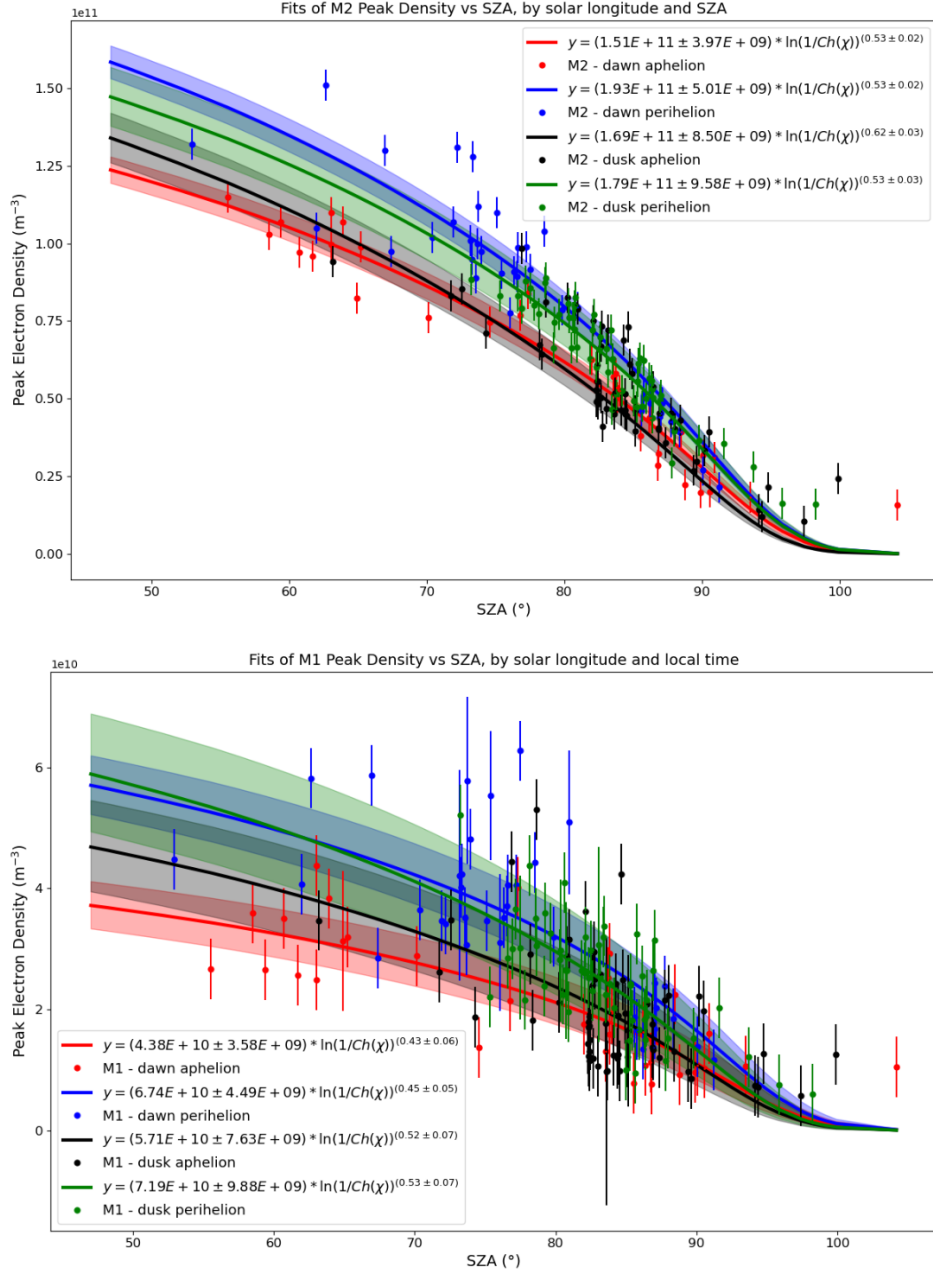


Figure 7: Fit for M1 (bottom) and M2 (top) peak densities for the four groups: dawn aphelion, dawn perihelion, dusk aphelion, and dusk perihelion. The results for the fit parameters are printed in the legend, and in Table 4 for clarity.

tween dawn perihelion and aphelion, consistently with the hypothesis of a more variable dawn ionosphere (Felici et al., 2022). For both the M1 and M2 layers, dawn perihelion is significantly higher in altitude and greater in density than dawn aphelion. For dusk aphelion and perihelion the difference is usually less extreme. Dusk perihelion is higher in density than dusk aphelion, but dusk aphelion is higher in altitude, particularly in the M1 layer.

Densities and altitudes of the M1 and M2 layers generally tend to be higher at perihelion, expected since when Mars is closer to the Sun, we expect higher solar flux to irradiate the atmosphere. However, densities and altitudes are lower than what Fallows et al. (2015) found, at solar maximum. Namely, corresponding to the solar minimum in the solar cycle, we find lower peak densities and lower peak altitudes for both the M1 and M2 layers (Withers et al., 2023).

Finally, as SZA increases the M1 and M2 peaks get farther in altitude from one another, yet closer in density.

5. Acknowledgements

The source for the sunspot number is WDC-SILSO, Royal Observatory of Belgium, Brussels. The Radio Occultation Science Experiment data used in this study is publicly available on the Planetary Data system. This work was supported by NASA under award number NNH1OCCO4C, LASP sub-contract 9500306435.

References

- Bougher, S.W., Brain, D.A., Fox, J.L., Gonzalez-Galindo, F., Simon-Wedlund, C., Withers, P.G., 2017. Upper Neutral Atmosphere and Ionosphere, in: Haberle, R.M., Clancy, R.T., Forget, F., Smith, M.D., Zurek, R.W. (Eds.), *The atmosphere and climate of Mars*. Cambridge University Press, pp. 405–432. doi:10.1017/9781139060172.014.
- Bougher, S.W., Engel, S., Hinson, D.P., Murphy, J.R., 2004. MGS Radio Science electron density profiles: Interannual variability and implications for the martian neutral atmosphere. *J. Geophys. Res.* 109, E03010, 10.1029/2003JE002154. doi:10.1029/2003JE002154.
- Chapman, S., 1931a. The absorption and dissociative or ionizing effect of monochromatic radiation in an atmosphere on a rotating Earth. *Proc. Phys. Soc.* 43, 26–45.

- Chapman, S., 1931b. The absorption and dissociative or ionizing effect of monochromatic radiation in an atmosphere on a rotating Earth. Part II. Grazing incidence. *Proc. Phys. Soc.* 43, 483–501.
- Fallows, K., Withers, P., Matta, M., 2015. An observational study of the influence of solar zenith angle on properties of the M1 layer of the Mars ionosphere. *J. Geophys. Res.* 120, 1299–1310. doi:10.1002/2014JA020750.
- Fallows, K., Withers, P., Matta, M., 2015. An observational study of the influence of solar zenith angle on properties of the M1 layer of the Mars ionosphere. *Journal of Geophysical Research: Space Physics* 120, 1299–1310. URL: <https://doi.org/10.1002/2014JA020750>, doi:doi:10.1002/2014JA020750.
- Felici, M., Withers, P., Smith, M.D., González-Galindo, F., Oudrhiri, K., Kahan, D., 2020. MAVEN ROSE Observations of the Response of the Martian Ionosphere to Dust Storms. *Journal of Geophysical Research* 125, e27083. doi:10.1029/2019JA027083.
- Felici, M., Withers, P., Vogt, M.F., Hensley, K.G., Andersson, L., 2022. Electron Densities in the Ionosphere of Mars: Comparison of MAVEN/ROSE and MAVEN/LPW Measurements. *Journal of Geophysical Research: Space Physics* 127, e2021JA030155. URL: <https://doi.org/10.1029/2021JA030155>, doi:<https://doi.org/10.1029/2021JA030155>.
- Flynn, C.L., Vogt, M.F., Withers, P., Andersson, L., England, S., Liu, G., 2017. MAVEN observations of the effects of crustal magnetic fields on electron density and temperature in the Martian dayside ionosphere. *Geophys. Res. Lett.* 44, 10,812–10,821. doi:10.1002/2017GL075367.
- Fox, J.L., Weber, A.J., 2012. MGS electron density profiles: Analysis and modeling of peak altitudes. *Icarus* 221, 1002–1019. doi:10.1016/j.icarus.2012.10.002.
- Fox, J.L., Weber, A.J., 2012. Mgs electron density profiles: Analysis and modeling of peak altitudes. *Icarus* 221. doi:10.1016/j.icarus.2012.10.002.
- Fox, J.L., Yeager, K.E., 2006. Morphology of the near-terminator martian ionosphere: A comparison of models and data. *Journal of Geophysical Research: Space Physics* 111. doi:10.1029/2006ja011697.

- Fox, J.L., Yeager, K.E., 2009. Mgs electron density profiles: Analysis of the peak magnitudes. *Icarus* 200. doi:10.1016/j.icarus.2008.12.002.
- Hantsch, M., Bauer, S., 1990. Solar control of the Mars ionosphere. *Planetary and Space Science* 38, 539 – 542. URL: <http://www.sciencedirect.com/science/article/pii/003206339090146H>, doi:[https://doi.org/10.1016/0032-0633\(90\)90146-H](https://doi.org/10.1016/0032-0633(90)90146-H).
- Hinson, D.P., Simpson, R.A., Twicken, J.D., Tyler, G.L., Flasar, F.M., 1999. Initial results from radio occultation measurements with Mars Global Surveyor. *J. Geophys. Res.* 104, 26997–27012.
- Jakosky, B.M., Lin, R.P., Grebowsky, J.M., Luhmann, J.G., Mitchell, D.F., Beutelschies, G., Priser, T., Acuna, M., Andersson, L., Baird, D., Baker, D., Bartlett, R., Benna, M., Bougher, S., Brain, D., Carson, D., Cauffman, S., Chamberlin, P., Chaufray, J.Y., Cheatom, O., Clarke, J., Connerney, J., Cravens, T., Curtis, D., Delory, G., Demcak, S., DeWolfe, A., Eparvier, F., Ergun, R., Eriksson, A., Espley, J., Fang, X., Folta, D., Fox, J., Gomez-Rosa, C., Habenicht, S., Halekas, J., Holsclaw, G., Houghton, M., Howard, R., Jarosz, M., Jedrich, N., Johnson, M., Kasprzak, W., Kelley, M., King, T., Lankton, M., Larson, D., Leblanc, F., Lefevre, F., Lillis, R., Mahaffy, P., Mazelle, C., McClintock, W., McFadden, J., Mitchell, D.L., Montmessin, F., Morrissey, J., Peterson, W., Possel, W., Sauvaud, J.A., Schneider, N., Sidney, W., Sparacino, S., Stewart, A.I.F., Tolson, R., Toubanc, D., Waters, C., Woods, T., Yelle, R., Zurek, R., 2015. The Mars Atmosphere and Volatile Evolution (MAVEN) Mission. *Space Science Reviews* 195, 3–48. URL: <https://doi.org/10.1007/s11214-015-0139-x>, doi:10.1007/s11214-015-0139-x.
- Kliore, A.J., Cain, D.L., Fjeldbo, G., Seidel, B.L., Sykes, M.J., Rasool, S.I., 1972. The atmosphere of Mars from mariner 9 radio occultation measurements. *Icarus* 17, 484–516. URL: <http://www.sciencedirect.com/science/article/pii/0019103572900140>, doi:[https://doi.org/10.1016/0019-1035\(72\)90014-0](https://doi.org/10.1016/0019-1035(72)90014-0).
- Mendillo, M., Withers, P., Hinson, D., Rishbeth, H., Reinisch, B., 2006. Effects of solar flares on the ionosphere of Mars. *Science* 311, 1135–1138. doi:10.1126/science.1122099.

- Montabone, L., Spiga, A., Kass, D.M., Kleinböhl, A., Forget, F., Millour, E., 2020. Martian year 34 column dust climatology from mars climate sounder observations: Reconstructed maps and model simulations. *Journal of Geophysical Research: Planets* n/a, e2019JE006111. URL: <https://doi.org/10.1029/2019JE006111>, doi:10.1029/2019JE006111.
- Morgan, D.D., Gurnett, D.A., Kirchner, D.L., Fox, J.L., Nielsen, E., Plaut, J.J., 2008. Variation of the martian ionospheric electron density from mars express radar soundings. *Journal of Geophysical Research: Space Physics* 113. doi:10.1029/2008JA013313.
- Němec, F., Morgan, D.D., Gurnett, D.A., Duru, F., 2010. Nightside ionosphere of mars: Radar soundings by the mars express spacecraft. *Journal of Geophysical Research: Planets* 115. URL: <https://doi.org/10.1029/2010JE003663>, doi:<https://doi.org/10.1029/2010JE003663>.
- Nielsen, E., Zou, H., Gurnett, D.A., Kirchner, D.L., Morgan, D.D., Huff, R., Orosei, R., Safaeinili, A., Plaut, J.J., Picardi, G., 2006. Observations of vertical reflections from the topside martian ionosphere. doi:10.1007/s11214-006-9113-y.
- Němec, F., Morgan, D.D., Gurnett, D.A., Duru, F., Truhlík, V., 2011. Day-side ionosphere of Mars: Empirical model based on data from the MAR-SIS instrument. *J. Geophys. Res.* 116, E07003, 10.1029/2010JE003789. doi:10.1029/2010JE003789.
- Pilinski, M., Andersson, L., Fowler, C., Peterson, W.K., Thiemann, E., Elrod, M.K., 2019. Electron Temperature Response to Solar Forcing in the Low-Latitude Martian Ionosphere. *Journal of Geophysical Research: Planets* 124, 3082–3094. URL: <https://doi.org/10.1029/2019JE006090>, doi:<https://doi.org/10.1029/2019JE006090>.
- Sánchez-Cano, B., Lester, M., Witasse, O., Brelly, P.L., Indurain, M., Cartacci, M., González-Galindo, F., Vicente-Retortillo, Á., Cicchetti, A., Noschese, R., 2018. Spatial, Seasonal, and Solar Cycle Variations of the Martian Total Electron Content (TEC): Is the TEC a Good Tracer for Atmospheric Cycles? *Journal of Geophysical Research: Planets* 123, 1746–1759. URL: <https://doi.org/10.1029/2018JE005626>, doi:<https://doi.org/10.1029/2018JE005626>.

- Smith III, F.L., Smith, C., 1972. Numerical evaluation of Chapman's grazing incidence integral $ch(x, x)$. *Journal of Geophysical Research (1896-1977)* 77, 3592–3597. URL: <https://doi.org/10.1029/JA077i019p03592>, doi:10.1029/JA077i019p03592.
- Tamburo, P., Withers, P., Dalba, P.A., Moore, L., Koskinen, T., 2023. Cassini radio occultation observations of saturn's ionosphere: Electron density profiles from 2005 to 2013. *Journal of Geophysical Research: Space Physics* 128, e2023JA031310. URL: <https://doi.org/10.1029/2023JA031310>, doi:<https://doi.org/10.1029/2023JA031310>.
- Withers, P., Felici, M., Hensley, K., Mendillo, M., Barbinis, E., Kahan, D., Oudrhiri, K., Girazian, Z., 2023. The ionosphere of Mars from solar minimum to solar maximum: Dayside electron densities from MAVEN and Mars Global Surveyor radio occultations. *Icarus* 393, 114508. URL: <https://www.sciencedirect.com/science/article/pii/S0019103521001834>, doi:<https://doi.org/10.1016/j.icarus.2021.114508>.
- Withers, P., Felici, M., Mendillo, M., Moore, L., Narvaez, C., Vogt, M.F., Oudrhiri, K., Kahan, D., Jakosky, B.M., 2020. The maven radio occultation science experiment (rose). *Space Science Reviews* 216, 61. URL: <https://doi.org/10.1007/s11214-020-00687-6>, doi:10.1007/s11214-020-00687-6.
- Withers, P., Fillingim, M.O., Lillis, R.J., Häusler, B., Hinson, D.P., Tyler, G.L., Pätzold, M., Peter, K., Tellmann, S., Witasse, O., 2012. Observations of the nightside ionosphere of Mars by the Mars Express Radio Science Experiment (MaRS). *J. Geophys. Res.* 117, A12307, 10.1029/2012JA018185. doi:10.1029/2012JA018185.
- Yao, M.J., Cui, J., Wu, X.S., Huang, Y.Y., Wang, W.R., 2019. Variability of the martian ionosphere from the maven radio occultation science experiment. *Earth and Planetary Physics* 3. doi:10.26464/epp2019029.